THERMAL CONDUCTIVITY OF FUSION SOLID BREEDER MATERIALS*

by

Yung Y. Liu and S. W. Tam**

Materials and Components Technology Division
Fusion Power Program
**Chemical Technology Division
ARGONNE NATIONAL LABORATORY
Argonne, Illinois 60439

June 1986

Distribution:
1. Y. Y. Liu
2. S. W. Tam
3. D. L. Smith
4. J. Rest
5-6. E. M. Stefanski
7-9. G. J. Hamilton

INVITED LECTURE to be given at the International Workshop on the Properties of Ceramics and Their Measurements, Soverato, Italy, September 22-27, 1986. To be published in Materials Chemistry and Physics.

*Work supported by the U.S. Department of Energy, Office of Fusion Energy, under contract W-31-109-Eng-38.

THERMAL CONDUCTIVITY OF FUSION SOLID BREEDER MATERIALS*

Yung Y. Liu

Materials and Components Technology Division, Fusion Power Program, Argonne National Laboratory, 9700 South Cass Avenue, Argonne, Illinois

S. W. Tam

Chemical Technology Division, Argonne National Laboratory, 9700 South Cass Avenue, Argonne, Illinois

ABSTRACT

Several simple and useful formulae for estimating the thermal conductivity of lithium-containing ceramic tritium breeder materials for fusion reactor blankets are given. These formulae account for the effects of irradiation, as well as solid breeder configuration, i.e., monolith or a packed bed. In the latter case, a coated-sphere concept is found more attractive in incorporating beryllia (a neutron multiplier) into the blanket than a random mixture of solid breeder and beryllia spheres.

INTRODUCTION

Lithium-containing ceramic materials (e.g., Li_2O, $LiAlO_2$, Li_2SiO_3, Li_4SiO_4, Li_8ZrO_6, etc.) are among the leading candidates considered as tritium breeding blanket materials for fusion reactors. The thermal conductivity of these materials is an important property to blanket design and performance because of the following reasons: (1) the dependence of blanket tritium breeding and heat generation capabilities on solid/nonsolid breeder volume fractions, (2) the temperature limits (upper and lower) within which solid breeder blankets are designed and operated, and (3) the dependence of tritium recovery and heat removal on solid breeder temperatures.

Several blanket configurations have evolved from past design studies [1-4]. Behind the first wall and within the structural wall boundaries, the

---

*Work supported by the U.S. Department of Energy, Office of Fusion Energy, under contract W-31-109-Eng-38.

solid breeder can take the form of a sintered monolithic block [1,2], sintered plates or pellets clad with structural materials [3,4], monosized sintered pebbles [5], or packing of high-density spheres known as sphere-pac [3]. To enhance tritium breeding, the blanket design often incorporates a neutron multiplier (such as beryllia) which exists in a zone either physically separated from the solid breeder or mixed with it as in the sphere-pac configuration.

There are two kinds of solid breeder thermal conductivities which are of concern here. The first is the usual thermal conductivity (k) of ceramic materials, which, in the temperature range of interest (350-1000°C), is dominated by phonon scattering and affected by materials inhomogeneities such as porosities. The second kind is the effective thermal conductivity (k_{eff}) of a packed bed in which heat transfer is accomplished by conduction through different phases (e.g., solid breeder, gas-filled space, neutron multiplier) of a heterogeneous material.

In this paper several simple and useful formulae for estimating the thermal conductivities (k and k_{eff}) of solid breeder materials are given which account for the effects of irradiation and solid breeder configuration (i.e., monolith or a packed bed). In the latter case, a hierarchical effective medium theory (HEMT) recently developed for granular materials has been applied to two packed bed configurations, one of which is a coated sphere concept. For purpose of illustration, only lithium oxide (Li_2O) and lithium aluminate (γ-$LiAlO_2$) are considered in this paper. The theories given below are general, and, therefore, readily applicable to other solid breeder materials.

THEORIES AND RESULTS

Sintered, Monolithic Solid Breeders

For many sintered ceramic materials (including Li_2O and $LiAlO_2$), the thermal conductivity data obtained for unirradiated samples can be represented very well by the following expression,

$$k(P) = k_o\, f(P), \ W/m\text{-}K \tag{1}$$

where k_o is the thermal conductivity of a theoretically dense solid breeder; f(P) is a porosity function (with P the fractional porosity) given by

$$k_o = \frac{1}{A + BT}, \tag{2}$$

$$f(P) = \frac{1 - P}{1 + \beta P}, \tag{3}$$

and A, B, and β are materials constants.

Equations (1) to (3) can be derived on rigorous theoretical grounds. According to the kinetic theory of gases, for example, an approximate but useful relationship for the phonon conductivity in an ideal lattice is

$$k_\ell = \frac{1}{3} Cv\Lambda_o, \quad \Lambda_o > a_o; \tag{4a}$$

or

$$k_{min} = \frac{1}{3} Cva_o, \quad \Lambda_o < a_o, \tag{4b}$$

where C is the heat capacity per unit volume, v is the phonon wave velocity in the solid, Λ_o is the attenuation length (or mean free path) of the lattice phonon waves, and k_{min} is the minimum lattice conductivity when the phonon wave length approaches atomic dimensions (a_o). In many solids k_{min} is not easily revealed because of melting and the other high-temperature conduction components (i.e., photons and electronic charge carriers). For γ-$LiAlO_2$, however, our recent work [6] indicated the existence of k_{min}.

For a non-ideal lattice with defects, phonon scattering will occur at these defects, in addition to phonon-phonon scattering. These defects in general change the mean free path rather than the other parameters in Eq. (4). The resulting mean free path Λ for a non-ideal lattice may then be written as

$$\frac{1}{\Lambda} = \frac{1}{\Lambda_o} + \sum_i \frac{1}{\Lambda_i}, \tag{5}$$

where Λ_i is the mean free path for phonon scattering by the ith type of defect initially present in an unirradiated material. It has been shown [7] by theory and confirmed by experiment that at temperatures significantly above the Debye temperature, $\Lambda_o \simeq \alpha/T$, where α is a constant characteristic of the material, and T is the temperature. The phonon-defect mean free path (Λ_i), on the other hand, is generally independent of temperature.

Replacing Λ_o in Eq. (4a) by Λ from Eq. (5) obtains the lattice thermal conductivity k_ℓ of unirradiated material, viz.,

$$k_\ell = \frac{1}{A + BT}, \tag{6}$$

which is identical in form to k_o given by Eq. (2) with

$$A = (3/Cv) \sum_i \frac{1}{\Lambda_i} \tag{7}$$

$$B = 3/Cv\alpha. \tag{8}$$

The theoretical derivation of Eq. (3) is due to Eucken [8]; the equation is sometimes referred as the Maxwell-Eucken relation. Another often used relation, the Loeb equation [9], also takes a simple form

$$f(P) = 1 - \alpha P, \tag{9}$$

where α is a materials constant and P is the fractional porosity. Eucken and Loeb have shown that the constants β and α are related to the shape and distribution of pores, to the ratio of thermal conductivities of solid versus gases in the pores, and to the emissivity of the pore surfaces. Thus, in principle one can compute thermal conductivities of unirradiated, sintered solid breeder materials from fundamental properties and details of the pore microstructure. In most cases, however, this was not done. Instead, the thermal conductivity data are usually correlated via Eqs. (1) to (3) to determine the constants A, B, and β. The values of these constants for Li_2O and γ-$LiAlO_2$ obtained by fitting the data will be given at the end of this section.

Other than tritium generation and nuclear heating, neutron irradiation also introduces additional defects (via radiation damage) into the solid breeder material. These defects may include displaced atoms, bubbles, voids, and cracks. They give rise to extra sources of phonon scattering, and the effect may be represented by additional mean free paths Λ_j for each of the jth type of defect introduced by irradiation. The total mean free path that determines the thermal conductivity of irradiated material may then be written as

$$\frac{1}{\Lambda_{irr}} = \frac{1}{\Lambda} + \sum_j \frac{1}{\Lambda_j}, \tag{10}$$

where Λ is given by Eq. (5).

If we designate the second term on the right-hand side of Eq. (10) as $\beta' = \sum_j \frac{1}{\Lambda_j}$, and further require that the lattice thermal conductivity of irradiated material (k_{irr}) be expressed in terms of the original unirradiated k_ℓ as

$$k_{irr} = \alpha_{irr}\, k_\ell, \tag{11}$$

it can be shown that the factor α_{irr} is given by

$$\alpha_{irr} = \frac{k_{irr}}{k_\ell} = \frac{1}{1 + \frac{\beta'}{A + BT}}. \tag{12}$$

As discussed in a previous publication [10], each of the constants A, B, and β' in Eq. (12) has a well-defined physical meaning. Constant A embodies

the mean free path for phonon-defect scattering; the defects are those initially present in an unirradiated material. Constant B embodies the mean free path for phonon-phonon scattering and is characteristic of the crystal structure of the material. Finally, constant β' embodies the mean free path for phonon-defect scattering; the defects are those produced by irradiation. Thus if k_ℓ and constants A, B, and β' are known, k_{irr} can be readily obtained as a function of temperature.

Experimental information on the Λ_j's for various defects are not available for solid breeders to permit direct use of Eq. (10). Consequently, we must resort to other methods for estimating β'. A simple procedure has formerly been developed [10] for this purpose, using data from irradiated dielectric insulator materials and UO_2. Briefly, all of the post-irradiation thermal diffusivity (hence thermal conductivity) measurements of these materials at room temperature showed a 10-75% reduction from their unirradiated values, followed by a saturation of reduction with respect to fast neutron fluence. The level of reduction in thermal conductivity depends on the crystalline structure and the ease with which defects can be formed by radiation damage. This connection should be obvious from earlier discussion, since irradiation produced defects represent additional scattering centers for phonons. Thus for damage resistant materials (e.g., $MgAl_2O_4$ and γ-$LiAlO_2$ with complex cubic and tetragonal crystal structures, respectively), the thermal conductivity degradation by neutron irradiation is expected to be less than that in UO_2 and Li_2O which have similar fluorite-type unit cells. Based on our survey of results from these irradiated dielectric materials, and by noting their crystalline structure similarity to solid breeders, the thermal conductivity reduction is assumed to be 50 and 25% for Li_2O and γ-$LiAlO_2$, respectively, after $0.5 - 2 \times 10^{26}$ n/cm^2 fast neutron exposure.

Recalling that $\alpha_{irr} = k_{irr}/k_\ell$ and with the reduction factors assumed above (α_{irr} equal to 0.5 and 0.75, respectively, for Li_2O and γ-$LiAlO_2$), the values of β' can be calculated by rearranging Eq. (12), i.e.,

$$\beta' = \left(\frac{1}{\alpha_{irr}} - 1\right)(A + BT), \tag{13}$$

and the final expression for k_{irr} after $0.5 - 2 \times 10^{26}$ n/m^2 is

$$k_{irr}(P) = \frac{k_\ell}{1 + \beta'/(A + BT)}\, f(P), \text{ W/m-K} \tag{14}$$

where f(P) is the porosity function given before for the unirradiated materials, and values of A, B, and β' are summarized in Table I for Li_2O and γ-$LiAlO_2$.

Table 1. Values of Constants in the Thermal Conductivity Expressions for Sintered Li_2O [11] and γ-$LiAlO_2$ [12]

Material	A	B	$\beta^{(a)}$	$\beta'^{(b)}$
Li_2O	2.2×10^{-2}	1.784×10^{-4}	$1.45 - 8 \times 10^{-4}T$	9.34×10^{-2}
γ-$LiAlO_2$	7.274×10^{-2}	4.67×10^{-4}	$1.45 - 8 \times 10^{-4}T$	8.65×10^{-2}

(a) The same expression of β (experimentally determined) for Li_2O is assumed for γ-$LiAlO_2$.

(b) Values are calculated from Eq. (13) at 400K for the assumed α_{irr} values.

Figures 1 and 2 show the calculated thermal conductivities for irradiated, sintered Li_2O and γ-$LiAlO_2$, respectively, at three densities (70, 85, and 98% dense). Compared to k_o of unirradiated solid breeders, the reduction of k_{irr} is larger at low temperatures, becoming less toward high temperatures.

Solid Breeder Packed Beds

One of the major problems in blanket temperature control with sintered solid breeders is the thermal conductance at breeder/structure interface. Accurate prediction of this interface conductance is very difficult, largely due to factors such as solid breeder cracking, cracked fragment relocation, sintering, creep, and swelling, which will alter the separation distance between solid breeder and structural materials (coolant tubes, for example) during blanket operation. The uncertainty in the interface conductance may be reduced by blending solid breeder particles in a packed bed configuration. In order to obtain high-density packing of solid breeders for adequate tritium breeding, relatively small spheres of different sizes must be used. Based on fission technology experience, the "sphere-pac" configuration has been chosen which should attain a solid packing fraction (SPF) of ~87% with three particle sizes (1200, 300, and 30 um diameters) and with particle density ~100% theoretical.

Heat transport in a system composed of close-packed spherical particles involves four distinctive processes: (1) lattice conduction, by which heat is transferred by phonons within the lattice of solid particles; (2) gas phase conduction, by which heat is transferred through the gas phase in the open spaces between particles and at gas-solid interfaces; (3) radiation heat transport, which is important at high temperatures and depends on surface emissivity; and (4) contact heat transport at solid particle interfaces, which

depends on contact pressure and surface roughness. Although each of the above heat transport processes is reasonably understood, the development of a model for the overall thermal conductivity (k_{eff}) of the system is complicated by the complex geometrical particle arrangement and the relative importance of each heat transport process. In the following, we shall devise a procedure for estimating k_{eff} of the sphere-pac solid breeders based on the data of UO_2 microspheres.

Moore et al. [13] investigated the effective thermal conductivities of powders with UO_2 or ThO_2 microspheres in several gases from 300 to 1300 K. Filled gas effects on k_{eff} were clearly indicated in the three-particle (1200, 300, and 25-45 μm nominal diameters) blended bed of UO_2 (SPF ~87%) in He, N_2, and Kr versus temperature at a gas pressure of 0.1 MPa (~1 atm). The relative magnitudes of k_{eff}'s reflect the different thermal conductivities of the three gases, with helium giving the highest k_{eff}. When the helium gas pressure was increased, Moore et al. [13] noted an increase in k_{eff}. The gas pressure effect on k_{eff} starts to level off, however, at a helium pressure of 0.6 MPa (~6 atm) such that further increase in pressure resulted in only marginal improvement of k_{eff}. Figure 3 shows the thermal conductivities for unirradiated UO_2; the solid lines for 98% and 85% TD sintered UO_2 represent data reported in Ref. [14] and the dash lines represent the k_{eff} data of Moore et al. obtained for sphere-pac UO_2 under helium pressures of 0.1-0.6 MPa.

To incorporate the different heat transport processes involved in a packed bed, a model for k_{eff} may be written as follows:

$$\lambda_{eff} = \sum_i \sum_j f_{ij} \lambda_j , \tag{15}$$

where $\lambda_{eff} = 1/k_{eff}$ is the overall thermal resistance of the system, λ_j is the thermal resistance of the jth heat transport process, and f_{ij} is a geometrical factor for the jth process reflecting a series/parallel combination of λ_j with other λ's.

In the analysis below, Eq. (15) is simplified to contain only two terms, i.e.,

$$\lambda_{eff} = \lambda_\ell + \bar{\lambda}_{g-s} , \tag{16a}$$

or

$$\frac{1}{k_{eff}} = \frac{1}{k_\ell} + \frac{1}{\bar{k}_{g-s}} , \tag{16b}$$

where subscripts ℓ and g-s denote lattice and gas/solid interface, respectively; f_{ij} is assumed to be one for all i and j. The new term $\bar{\lambda}_{g-s}$ (or $1/\bar{k}_{g-s}$), in a sense represents the sum of the thermal resistances from all processes except that due to lattice conduction. From the thermal conductivity data of the sphere-pac as well as the high-density, sintered UO_2, one can calculate $\bar{\lambda}_{g-s}$ directly from Eq. (16a) as a function of temperature and helium fill-gas pressure. The results are summarized in Table II.

Table II. Values of $\bar{\lambda}_{g-s}$ $(W/m-K)^{-1}$ Calculated from Eq. (16) and the UO_2 Data.

Temperature (K)	Helium Pressure (MPa) 0.1	0.2	0.6
500	0.357	0.257	0.199
600	0.389	0.288	0.204
700	0.414	0.308	0.208
800	0.450	0.335	0.217
900	0.457	0.336	0.222
1000	0.479	0.349	0.235

The key assumption in the above procedure for estimating k_{eff} of sphere-pac solid breeders is that the $\bar{\lambda}_{g-s}$ values given in Table II are applicable, even though they were derived from the UO_2 data. The assumpton also implies that the details involved in the gas-solid heat transport and in the contact resistance between particles are the same for these different sphere-pac systems. For the UO_2 experiment [13] and for a sphere-pac blanket module where external constraints are relatively small, the contact heat transport is probably of secondary importance, compared to heat transport at gas-solid interfaces.

Near the solid particle contact region, the distance between the spheres becomes smaller than the mean free path of gas molecules. Rarefied gas properties are therefore expected in this region. Heat transfer under such conditions is often represented in terms of a "temperature jump distance" at the gas/solid boundaries [15]. This distance depends on the accommodation coefficient for the gas and solid surfaces, and on several gas properties (e.g., thermal conductivity, viscosity, specific heat, etc.). While the latter helium gas properties are identical in the sphere-pac UO_2 and solid breeder systems, the accommodation coefficients can be quite different, as

they involve both gas and solid. Kennard [15] gives a simple model in which the molecular masses of the gas and solid completely determine the accommodation coefficient. The model predicts a much lower accommodation coefficient (~0.33) for UO_2/He than those for Li_2O/He (~0.21) and γ-$LiAlO_2$/He (~0.11). This would result in a larger temperature jump distance for UO_2/He than for solid breeders/He. Since the temperature jump distance represents incomplete heat transfer near the gas/solid interface, the larger the temperature jump distance, the less effective the heat transfer. This means that the gas-phase heat transport contribution to k_{eff} will be more for UO_2 than for solid breeders. On this basis the estimated k_{eff} for sphere-pac solid breeders may be conservative (i.e., lower than the actual values). However, it should also be noted that other factors (such as surface roughness) can significantly influence the accommodation coefficient.

Assuming that $\bar{\lambda}_{g-s}$ values given in Table II are applicable to sphere-pac solid breeders, the k_{eff} of sphere-pac Li_2O and γ-$LiAlO_2$, with or without irradiation, can be estimated from Eqs. (16) with k_ℓ calculated from Eqs. (2) and (12) for high-density, sintered solid breeders. The results are displayed in Figures 4 and 5 for sphere-pac Li_2O and γ-$LiAlO_2$, respectively. Compared to the unirradiated k_{eff}, the irradiated k_{eff} is 12 to 19% lower for Li_2O and 6 to 12% lower for γ-$LiAlO_2$ at 1000 K. Part of the differences in percent reduction resulted from the different reduction factors (50 versus 25%) assumed for Li_2O and γ-$LiAlO_2$; part also depends upon the relative magnitudes of λ_ℓ and $\bar{\lambda}_{g-s}$, i.e.,

$$\frac{\Delta k_{eff}}{k_{eff}} = 1 - \frac{1 + (\lambda_\ell/\bar{\lambda}_{g-s})}{(1 + F\lambda_\ell/\bar{\lambda}_{g-s})} \tag{17}$$

where k_{eff} is that of the unirradiated system, Δk_{eff} is the difference of k_{eff} between unirradiated and irradiated system, and F is the reduction factor of k_ℓ due to irradiation. Equation (16) shows that when $\bar{\lambda}_{g-s} >> \lambda_\ell$, k_{eff} will be dominated by $\bar{\lambda}_{g-s}$. Irradiation effects, which change only λ_ℓ, will be minor on k_{eff}. The k_ℓ of Li_2O is a factor of ~2 higher than that of γ-$LiAlO_2$, so that λ_ℓ of Li_2O is ~1/2 of that of γ-$LiAlO_2$. Since the same $\bar{\lambda}_{g-s}$ is used for both systems, this means λ_ℓ is relatively more important to λ_{eff} (and k_{eff}) for γ-$LiAlO_2$ than Li_2O. The same kind of argument may be used to explain the thermal conductivity results of γ-$LiAlO_2$ in the TRIO experiment [16]. Since the γ-$LiAlO_2$ pellets in TRIO contain a rather high fraction (~0.35) of porosity and their microstructure remain unchanged during irradiation, the thermal resistance, λ_p, due to the as-fabricated pores should remain large (if not dominant) during irradiation. Irradiation-induced defects will increase λ_ℓ

somewhat, but if λ_ℓ is substantially lower than λ_p, irradiation effects on thermal conductivity of low-density (but microstructurally stable) material should be minor.

Coated Sphere Concept

At equivalent volume fractions of solid breeders in the blanket, Figs. 1-2 and Figs. 4-5 show that the k_{eff}'s of the sphere-pac materials are generally a factor of 2 to 3 lower than the k's of the sintered materials. Concepts that can lead to enhancement of k_{eff} would, therefore, be of definite benefits. Consideration of the blanket tritium breeding ratio (i.e., >1 for tritium self sufficiency) implies that for most solid breeders the addition of a neutron multiplier (e.g., beryllium or beryllia) is a necessity. Since beryllium and beryllia have much higher thermal conductivities (115 and 87 W/mK for Be and BeO, respecitvely at 700 K) than that of the solid breeders (6.5 and 3.6 W/mK for Li_2O and γ-$LiAlO_2$, respectively at 700 K), a potential exists for enhancing the k_{eff} of a packed bed in which solid breeder is mixed with a higher conductivity neutron multiplier.

There are two ways by which a neutron multiplier (taken to be BeO) may be incorporated into a sphere-pack bed of solid breeder (taken to be γ-$LiAlO_2$). One is to mix BeO spheres similar to those of γ-$LiAlO_2$ in a random fashion; the other is by coating the γ-$LiAlO_2$ spheres with the right amount of BeO and packing the resulting compositie spheres in the usual manner. It turns out that the latter coated-sphere configuration gives a k_{eff} considerably higher than that of the mixed-sphere configuration of the same BeO/γ-$LiAlO_2$ composition. The basis of this result will be briefly described below, with the aid of a recently developed hierarchical effective medium theory (HEMT) for finely divided materials [17].

The basic idea of HEMT relies upon successive embedding of larger spheres into an effective medium of smaller spheres in a self-consistent manner. For the present situation the HEMT needs to be generalized to take into account the presence of two material components, the lithium ceramic breeder and the neutron multiplier material. Furthermore, these two components are arranged in two different configurations, namely, the coated-sphere configuration (CSC) and the mixed-sphere configuration (MSC).

The thermal conductivity k_s of a coated sphere can be calculated as follows [18]

$$k_s = k_c[2k_c + k_i + 2n(k_i - k_c)]/[2k_c + k_i - n(k_i - k_c)], \qquad (18)$$

where

k_c = thermal conductivity of the coated layer,

k_i = thermal conductivity of the interior component under the coated layer,

n = volume fraction of the interior component.

Using Eq. (18) and treating the coated spheres as if they were made up of one material component only, the HEMT can be applied in a straightforward manner.

A modification of the above approach is necessary for the mixed-sphere configuration since there are now two types of unit cells. One is given by a γ-$LiAlO_2$ sphere surrounded by its gaseous environment, the other being a BeO sphere surrounded by its own gaseous environment. The effective thermal conductivities of these two unit cells must be calculated separately, and neither of these two can necessarily be considered as a continuous medium. In a natural manner, however, this allows application of Bruggeman's symmetrical effective medium theory [18] to compute the k_{eff} of this sphere-pac bed with random mixing of γ-$LiAlO_2$ and BeO spheres.

Figure 6 shows the calculated k_{eff} of a sphere-pac bed in the mixed-sphere as well as the coated-sphere configuration. The BeO composition is the same in both cases at 20%. Notice that k_{eff} (CSC) is significantly above k_{eff} (MSC). An enhancement factor ε defined as

$$\varepsilon = \frac{k_{eff}(CSC) - k_{eff}(MSC)}{k_{eff}(MSC)} ,$$

and plotted also in Fig. 6 is seen to vary from ~70% at 500K to ~30% at 1500K.

The results shown in Fig. 6 were obtained under a helium pressure of 0.1 MPa. In powder-like systems such as the sphere-pac beds, the regions close to the points of contact between particles can have linear dimension that is comparable to or smaller than the mean free path of the gas. In that case, significant pressure dependence of thermal conductivity can be expected. Figure 7 shows the results obtained from the generalized HEMT for the two sphere-pac configurations between a range of helium pressures (0.1 - 0.9 MPa) at 1000K. A modest change in helium gas pressure is seen to result in a significant enhancement of the effective thermal conductivity. The CSC system is also more sensitive to gas pressure than the MSC system. Within the range of gas pressure considered, it is obvious that the k_{eff} of the CSC system has not yet reached near saturation, unlike the case of MSC.

DISCUSSIONS AND CONCLUSIONS

There are reasons to believe that the thermal conductivity estimates given in this paper will be somewhat conservative, i.e., lower than the actual values. The β' in Eq. (12) assumed constant in this work will in fact

decrease with increasing temperature due to more effective annealing of the damage induced by irradiation. Thermal and radiation-enhanced sinterings could further improve the thermal conductivities at high temperatures.

Thermal stability tests [19], conducted for 8 h at 1173 K on 85%-dense Li_2O and γ-$LiAlO_2$, showed that the latter is stable, but the grains in Li_2O grew from a 6-μm average to 60-100 μm. Since grain growth generally occurs concurrent with sintering, pore closure seems highly likely in Li_2O over a relatively short period at 1173 K. The Li_2O grain growth results in the FUBR-1A irradiation experiment [20] indicated a factor of 2 growth in grain size at 973 K, and a factor of 6 growth at 1173 K, both after a fast neutron exposure of $<6.8 \times 10^{25}$ n/m^2. In the same experiment, the γ-$LiAlO_2$ exhibited essentially no grain growth, even though the starting grain size (<1 μm) is considerably smaller than that of Li_2O. In the OG-5 irradiation experiment [21], the major fraction of pores in the low-density (68%-dense) Li_2O became closed pores for irradiation temperatures >1123 K after a fast fluence of 2×10^{25} n/m^2; the pores remained open for irradiation temperatures <1023 K. The pores in the low-density (70% TD) $LiAlO_2$, on the other hand, remained open up to 1273 K, after a fast neutron exposure of 2.7×10^{25} n/m^2. Effects of capture versus fast-neutron displacement damages on sintering are not easily discernible in the OG-5 experiment, primarily because highly depleted ^6Li was used which burned up at much lower fluences.

The various ex-reactor and in-reactor results indicate that the grain growth and sintering are more likely to occur in Li_2O (>1023 K) than in γ-$LiAlO_2$ (>1273 K). Besides the temperature dependence, solid-state sintering generally increases with time t at temperature ($\propto t^m$, $m < 1$), and with decreasing particle size r ($\propto r^{-n}$, $n < 1$). For the sphere-pac solid breeders, stage-I sintering (i.e., neck growth) appears likely to occur at sufficiently high temperatures (>0.6 T_m where T_m is the melting point at 1706 and 1883 K, respectively, for Li_2O and γ-$LiAlO_2$) between the fine particles (i.e., with 30-μm diameters). The net result of this neck growth is to reduce the contact resistance between particles, resulting in an increase of k_{eff} at high temperatures. Quantitative assessment of the sintering effect on k_{eff} cannot be made at this time because of the lack of solid-breeder sintering data.

Given two heterogeneous systems whose constituents and compositions are identical, they can still possess significantly different properties if the constituents in the two systems are arranged in different geometrical configurations. The point has been well brought out by our HEMT calculations of k_{eff} for a BeO-coated γ-$LiAlO_2$ sphere-pac system. By maximizing the long-range connectivity of the better conductive component (i.e., BeO) in the system, we have shown quantitative enhancement of k_{eff} of the coated-sphere

concept over that of a random mixture of solid breeder and neutron multiplier spheres.

REFERENCES

1 C. Baker et al., Argonne National Laboratory report, ANL/FPP-80-1, 1980.

2 M. A. Abdou et al., Argonne National Laboratory report, ANL/FPP-82-1, 1982.

3 D. L. Smith et al., Argonne National Laboratory report, ANL/FPP-84-1, 1984.

4 C. Baker et al., Argonne National Laboratory report, ANL/FPP-85-2, 1985.

5 K. Sumita and Y. Seki, Fusion Technol., 8, No. 1 (1985) 501.

6 S. W. Tam et al., J. Nucl. Mater. 133&134 (1985) 234.

7 P. G. Klemens in S. Flugge (ed.), Encyclopedia of Physics, Springer-Verlag, Berlin, 1956, Vol. 14, p. 198.

8 A. Eucken, Forsch. Gebiete Ingenieurw., B3, Forschungsheft No. 353 (1932) 16.

9 A. L. Loeb, J. Am. Ceram. Soc., 37, No. 2 (1954) 96.

10 Y. Y. Liu and S. W. Tam, Fusion Technol., 7 (1985) 399.

11 T. Takahashi and T. Kikuchi, J. Nucl. Mater. 91 (1980) 93-102.

12 G. W. Hollenberg, presented at 84th Annual Mtg. of Am. Cer. Soc., Cincinnati, Ohio, May 3-5, 1982.

13 J. P. Moore et al., Oak Ridge National Laboratory report, ORNL/TM-8196, 1982.

14 D. Hagrman et al., Nuclear Regulatory Commission report, NUREG/CR-0491, TREE-1280, Rev. 1, 1980.

15 E. H. Kennard, Kinetic Theory of Gases, McGraw-Hill, New York, 1953, p. 291.

16 R. G. Clemmer et al., Argonne National Laboratory report, ANL-84-55, 1984.

17 S. W. Tam and C. E. Johnson, to be published in J. Nucl. Mater.

18 R. Landauer in J. C. Garland and D. B. Tanner (eds.), Electrical Transport and Optical Properties of Inhomogeneous Media, Am. Inst. Phys., New York, 1978, p. 2.

19 C. N. Wilson and G. W. Hollenberg, US Department of Energy report, DOE/ER-0113/2, 1983, p. 23.

20 G. W. Hollenberg, J. Nucl. Mater. 133&134 (1985) 362.

21 L. Yang et al., J. Nucl. Mater. 103&104 (1981) 585.

List of Figures

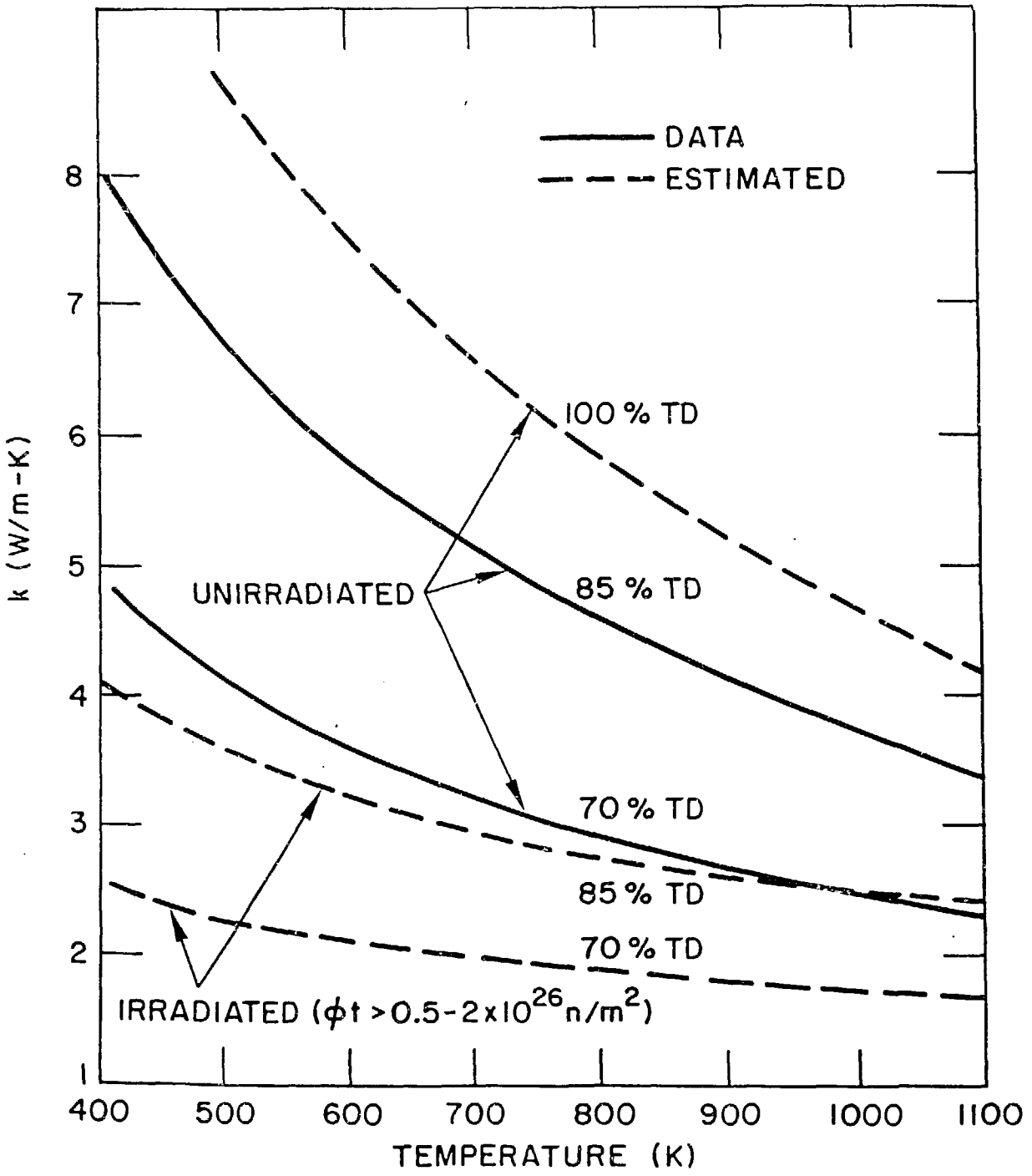

Fig. 1. Thermal conductivity of sintered Li_2O.

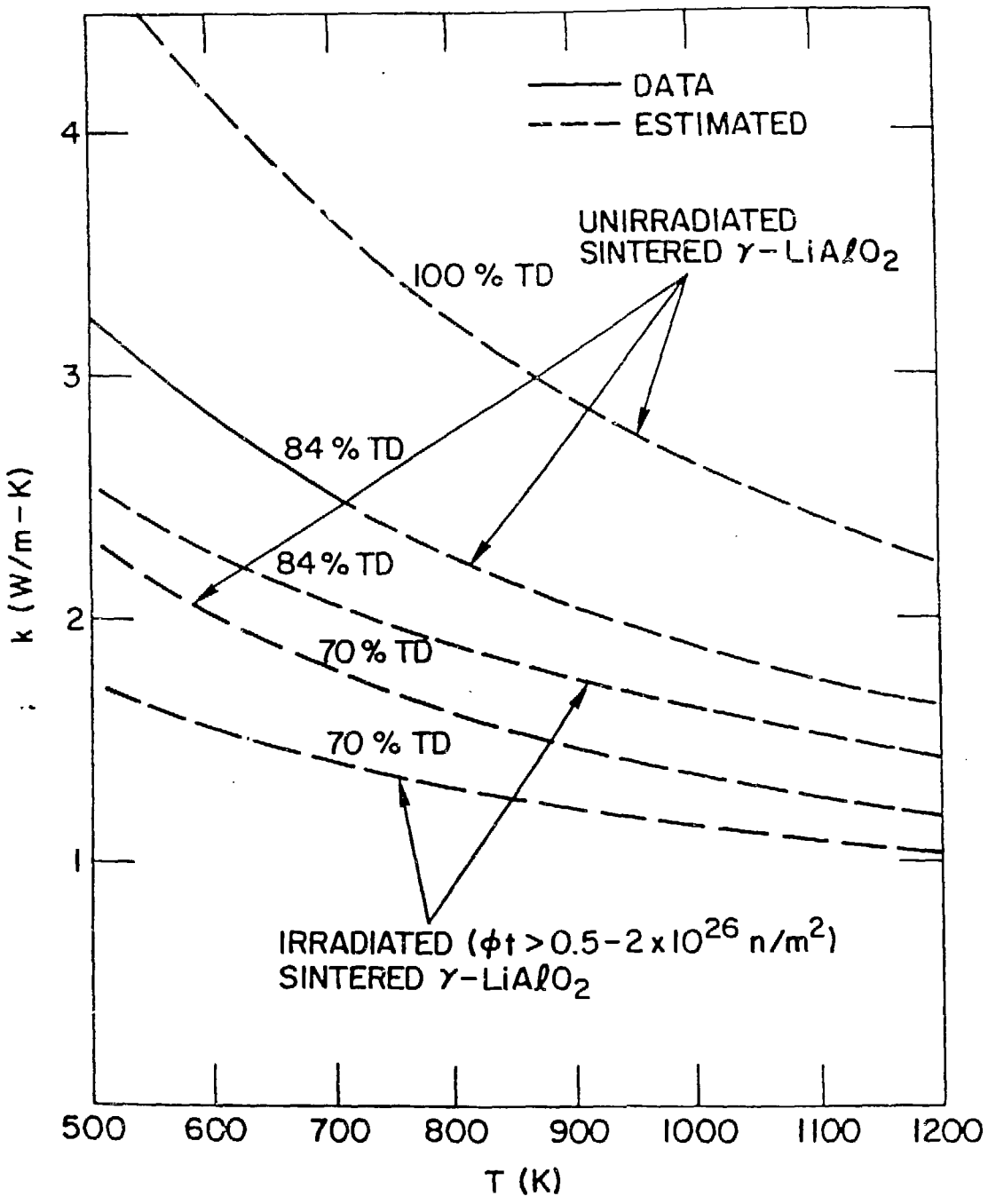

Fig. 2. Thermal conductivity of sintered γ-$LiAlO_2$.

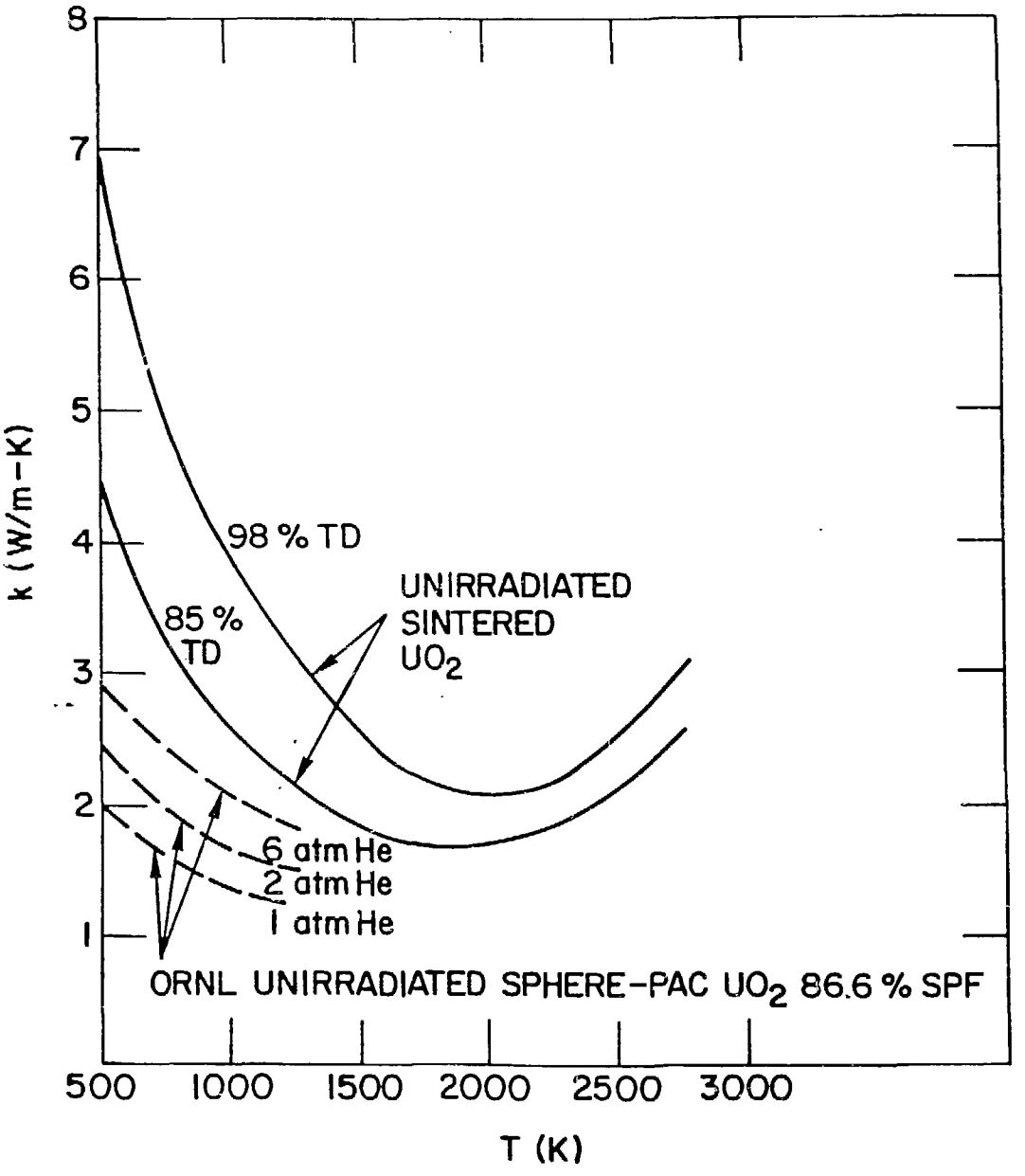

Fig. 3. Thermal conductivity for unirradiated, sintered, and sphere-pac UO_2 versus temperature and helium fill gas pressure.

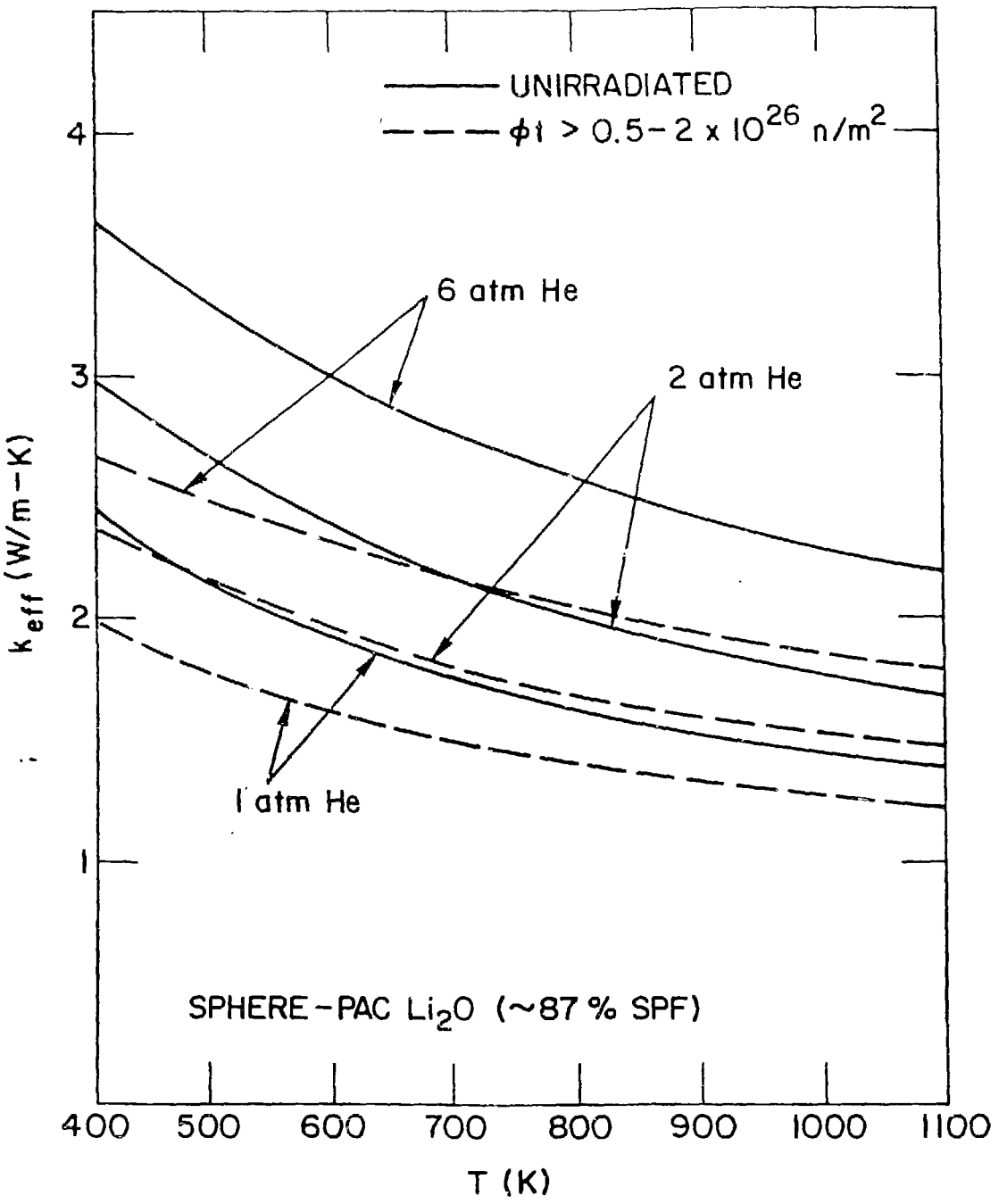

Fig. 4. Thermal conductivity of sphere-pac Li_2O.

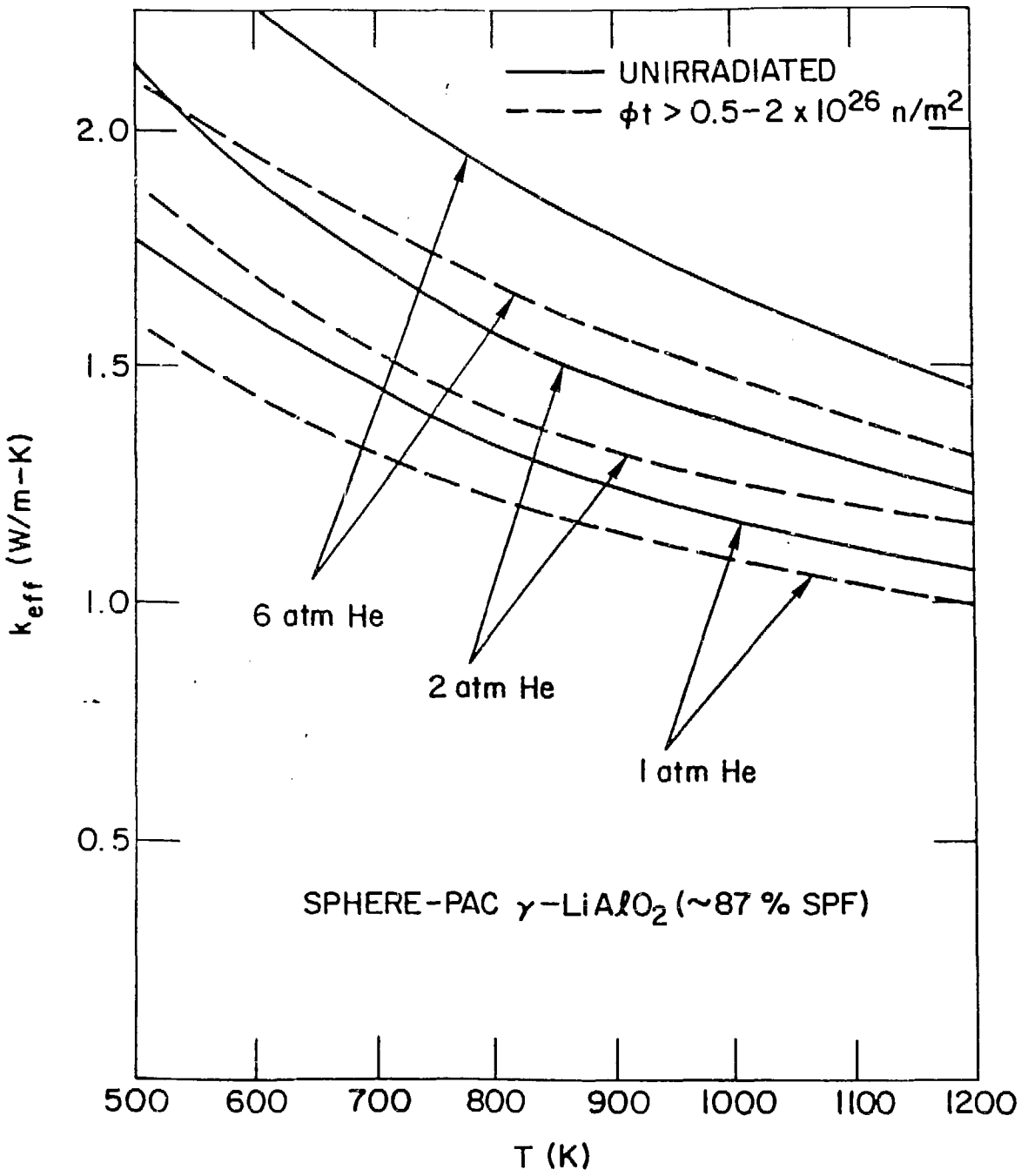

Fig. 5. Thermal conductivity of sphere-pac γ-$LiAlO_2$.

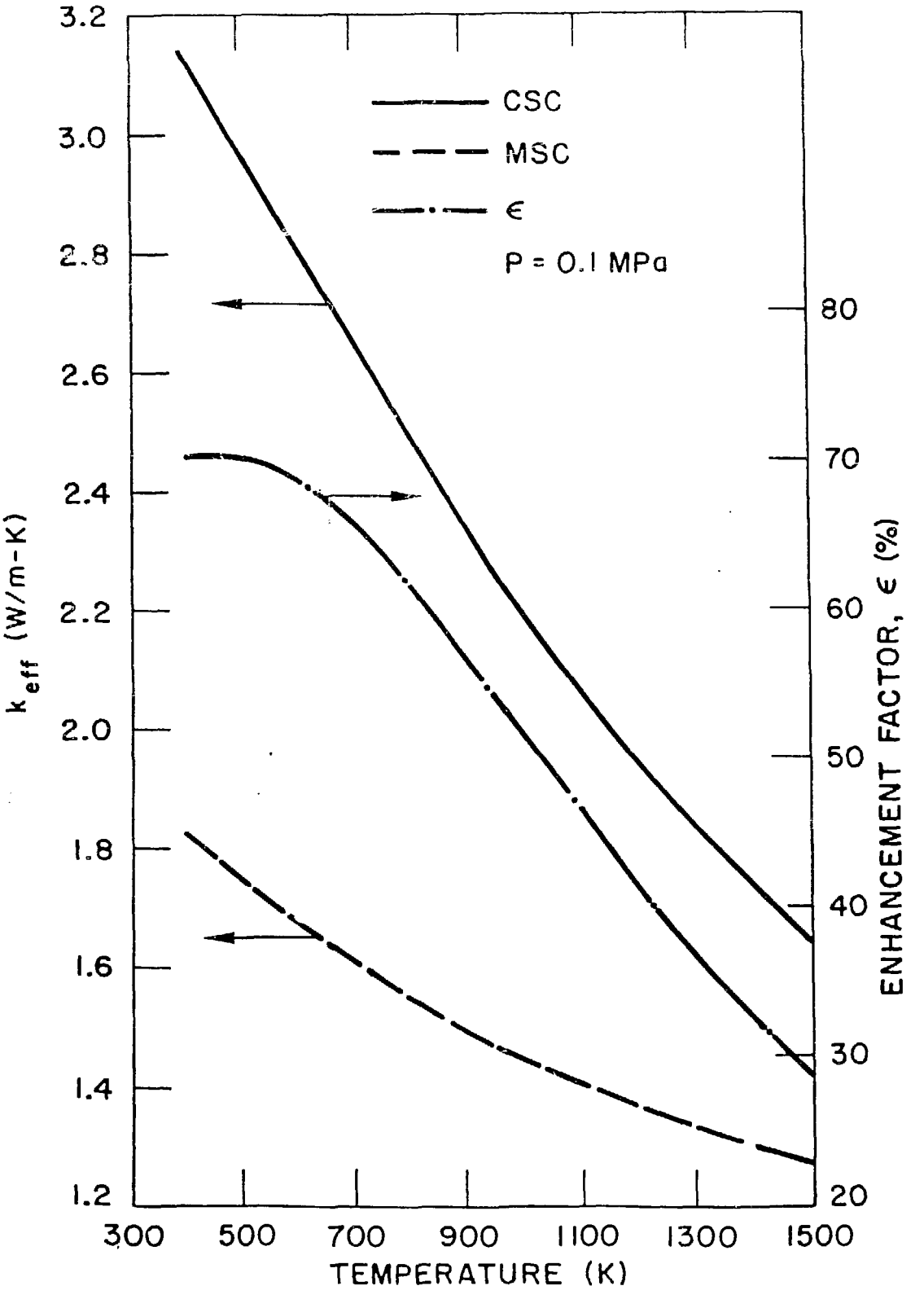

Fig. 6. Thermal conductivity of sphere-pac mixture of γ-$LiAlO_2$ and BeO versus temperature. (MSC: mixed sphere configuration; CSC: coated sphere configuration.)

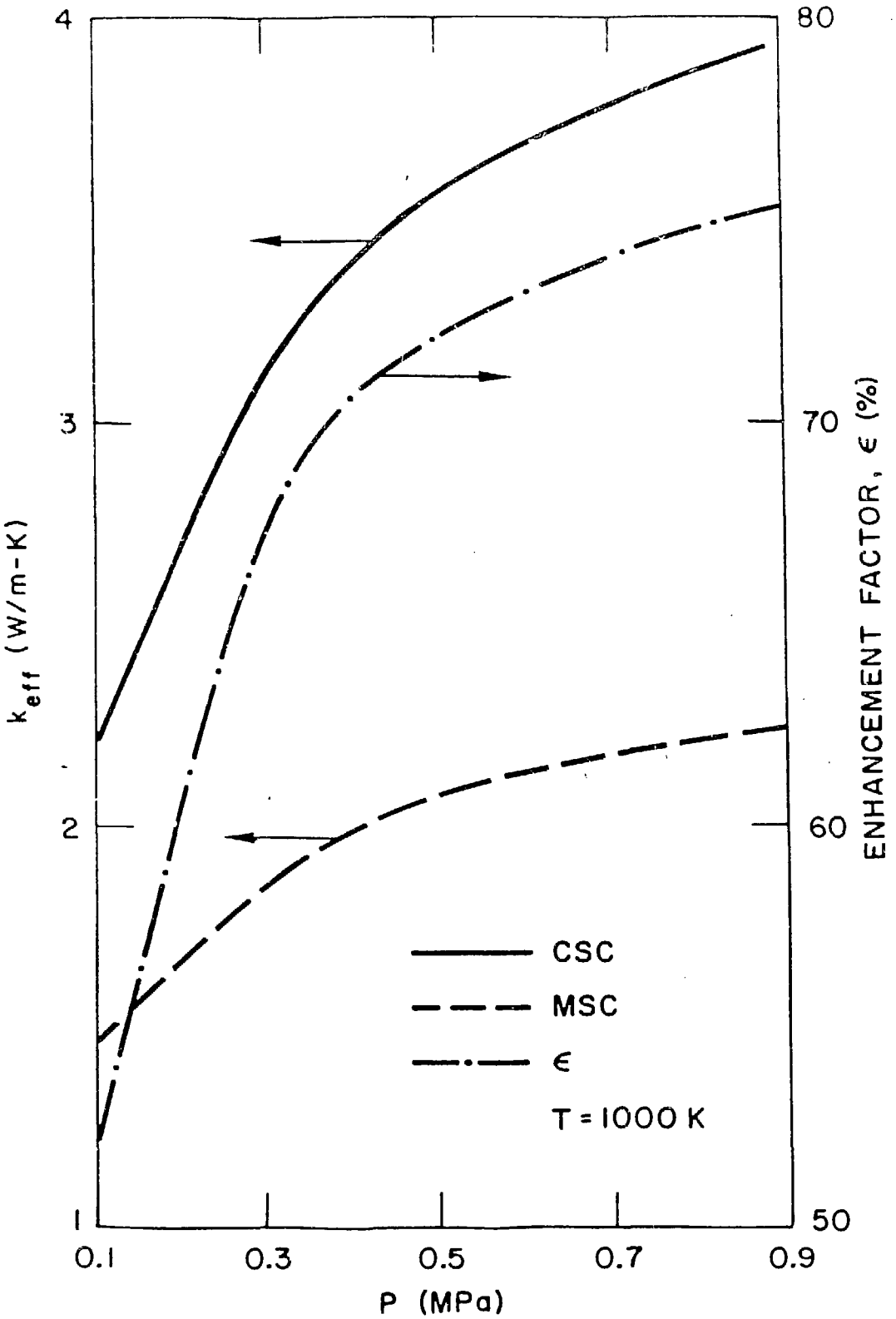

Fig. 7. Thermal conductivity of sphere-pac mixture of γ-$LiAlO_2$ and BeO versus helium gas pressure (MSC: mixed sphere configuration; CSC: coated sphere configuration.)